KSME

Springer

Journal of Mechanical Science and Technology 34 (9) 2020

Original Article
DOI 10.1007/s12206-020-0836-6

Keywords:
· Condensation coefficient
· Monte Carlo simulation
· Phase-change phenomena
· Nanofluidics

Correspondence to:
Minsub Han
mhan@inu.ac.kr

Citation:
Han, M. (2020). Mass exchange at liquid-solid interface: a molecular simulation scheme applied to evaporation phenomena. Journal of Mechanical Science and Technology 34 (9) (2020) 3855~3862.
http://doi.org/10.1007/s12206-020-0836-6

Received February 8th, 2020
Revised May 29th, 2020
Accepted June 22nd, 2020

† Recommended by Editor
Yong Tae Kang

Mass exchange at liquid-solid interface: a molecular simulation scheme applied to evaporation phenomena

Minsub Han

Department of Mechanical Engineering, Incheon National University, Incheon 22012, Korea

Abstract A numerical technique is presented that enables mass exchange at the liquid–solid interface region in a molecular simulation. Particles can be inserted and deleted in the solid region where interaction between the fluid and solid atoms is temporarily inactivated during the process. A simple momentum-increase scheme drives the inserted particles against the unfavorable free energy. The technique is efficient and stable for insertion of particles into dense and inhomogeneous regions. The thin film and sessile-drop evaporation phenomena are then investigated using the proposed technique that allows steady-state simulations. The evaporation coefficients for the nanoscale thin film and contact line were accurately and reliably measured. The evaporation coefficient near the contact line shows a discrepancy compared to that far from the contact line.

1. Introduction

The simulation of a molecular system open for mass exchange is quite useful in the investigation of a wide range of scientific and technological problems. The periodic boundary condition (PBC) is widely used in molecular simulations; it can consider a periodic infinite space with computational resources of a limited size [1, 2]. The PBC is, however, insufficient to apply to problems with non-periodic geometry and global gradients with critical properties [3-5]. A mass exchange technique can maintain the non-periodic condition at the boundary. More general usage is on the systems in open contact with a large reservoir, the subject of grand canonical simulations where the mass is exchanged freely with the reservoir of constant chemical potential [3, 6-8]. Another field of growing importance is the multiscale simulation, which seamlessly connects properties such as mass at the boundary between simulation methods of different scales [9-11].

Significant efforts in the last decade were devoted to developing a robust and efficient method to enable mass exchange in molecular simulations. Among the mass-exchange processes, the trickiest operation is the particle-insertion into a dense phase, like liquid. Any randomly chosen insertion position easily overlaps the positions of existing molecules. The strong repulsive force then destabilizes the integration of equations of motion in the simulation. An early attempt to overcome the situation used the method of pre-scanning the potential field [12]. The successful insertion probabilities are assigned to the candidate positions according to the field. This helps to avoid the high potential positions and increases the success rate. The scanning operation still demands a significant computational load because it is performed every few steps according to the evolution speed of the potential field. A more elaborate insertion scheme called USHER is later introduced [13]. USHER uses the local energy landscape information and searches for the optimal position for insertion by the steepest descent iteration. USHER shows excellent performance for small molecules such as argon or water. Borg et al. later suggested an insertion protocol, called FADE, that can easily be applied to macromolecules such as 10-bead-long linear polymer melts and Buckminster fullerene [14].

FADE requires a time-varying weighting factor whose parameters must be tested for a

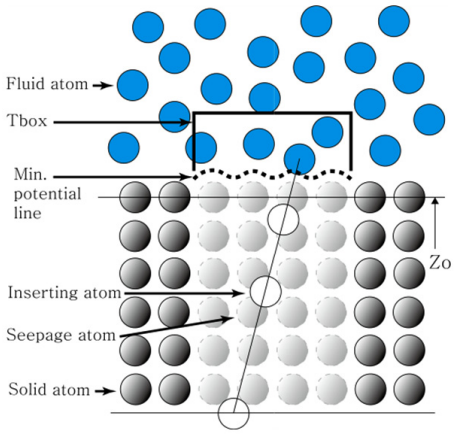

Fig. 1. Schematic of the insertion process. If z < Zo or z < Min.-potential-line (or the solid interaction force is positive), apply SB condition. Otherwise, apply attractive potential.

specific molecular system. Another notable method is to apply a soft repulsive potential in a buffer zone between the main simulation region and the boundary. A smooth transition between the strong and soft repulsive potentials is facilitated by the method called AdResS [15]. More recently, a scheme for insertion and deletion operations called PIE was introduced [16]. PIE does not require pre-determined parameters and is virtually stable. The PIE scheme is based on an extended Hamiltonian where an extra coordinate is introduced to relieve the strong repulsive force, and insertions into dense phases are demonstrated for large macromolecules such as linear polymer, nanotube, and nano-sized particles.

One unexplored area in these remarkable progresses is the insertion and deletion of particles at the solid–liquid interfacial region. These mass-exchange techniques are demonstrated for the bulk phase. Insertions at the interface are especially useful in simulating phenomena where a fluid system is bounded by different phases or materials. For example, when a liquid drop on a solid substrate evaporates, the drop decreases in size with time. Simulation of this phenomenon produces transient data that normally contains a significant fluctuation level that resists quantitative analysis. If a mass source is located inside the drop, the phenomenon becomes steady and significant data set samples are obtained for a specific state. This will produce more reliable data that requires less modeling effort. The mass exchange operations need to be as far from the liquid–vapor interface as possible. Otherwise, the operations may disrupt the phenomena of interest at the free surface. The least disruptive method is to locate the operations at the liquid–solid interfacial region. However, the insertion and deletion operations through the liquid–solid interface is a challenging task different from those in bulk. The liquid is denser and more structured and solid atoms exist. Thus, the target region is inhomogeneous in density and material.

The insertion technique at the liquid–solid interface immediately contributes to the analysis of the mass and energy transfers at the vapor-liquid interface during evaporation and condensation which are crucial phenomena in many science and technology fields [17-21]. One of the key aspects for understanding and modeling the phenomena is the interfacial kinetic boundary condition (KBC), which prescribes how the molecules interact with the interface. Net mass and energy fluxes are determined accordingly. An accurate accommodation coefficient has been investigated using the simulation on the liquid–vapor interface [22, 23]. The evaporating drop on a solid substrate has been widely studied [18]. The evaporative mass flux near the contact line is an important property because it shows a significant increase on a high-energy substrate. It is usually assumed that KBC does not change near the contact line; however, to the best of the author's knowledge, this has not yet been confirmed.

This paper presents a simulation method to exchange particles at the solid–liquid interface. This method can provide a mass source or sink inside the liquid and should be quite useful in simulating the fluid system bounded by different phases or materials. The use of this method is demonstrated by investigating the liquid drop and thin film evaporation phenomena on a solid substrate. The distributions of evaporation rate and coefficient throughout the liquid–vapor interface are quantitatively investigated; these are the steady-state simulation results obtained using the insertion method.

2. Theory

When a particle is inserted into a liquid phase in contact with a solid substrate, the initial particle location is chosen as far from the interface as possible so that strong interactions with the remaining liquid particles are relieved and the initial insertion step remains stable. However, the initial insertion location overlaps the solid region. Therefore, the interactions, especially repulsive ones, between the inserted particle and the solid atoms must be relieved. This is made possible by introducing solid atoms having a different, more stable, repulsive potential. This solid will be called a seepage solid that is distinguished from the real solid (see the blurred particles in Fig. 1). When two atoms interact with each other, there are two interaction types, attractive and repulsive. The former is soft and long-ranged, and the latter is strong and short-ranged. The repulsive force originates from the overlap of electron clouds and is a dominant factor in determining the liquid structure. The force also quickly destabilizes the insertion operation of an ill-chosen location. The basic idea of the scheme introduced in this study is to replace the repulsive potential of the solid, interacting with the inserted atom with a more stable potential, which will be called "soft bounce" (SB). Soft bounce is most straightforwardly introduced in the interaction context with a wall (Fig. 2). When a particle interacts elastically with a hard wall, there are three simple ways to implement the elastic interaction in the molecular simulation. Because the equations of motion are integrated in a finite time step, the wall interaction is applied to the particle only when the particle passes the wall location and becomes out of bounds (②" in Fig. 2). The case of (①→②→③) is the

most accurate realization of the interaction. However, the correct position ② is a distance from the wall and can be occupied by other particles and become unstable. Locating the particle right at the wall (②') would be a less accurate but more stable choice. Particles can still be nearby and thus be disrupted by the locating effort. Not changing the out-of-bound particle location (②") would be the most stable condition, while least accurate. The three interactions types all converge as the time step approaches zero. In summary, while the first two methods may be more accurate, they have the potential to disrupt the existing particles near the boundary. The third is virtually stable because it does not change the particle position at all, only the normal velocity sign, which will be called SB interaction. By using the SB interaction, a potential for the seepage solid is modeled. In Fig. 3, the seepage-solid potential is illustrated. The seepage-solid potential is similar to the well-known hard sphere with soft attraction where the repulsive part is simplified with a hard wall that enforces an exact wall position such as ②' in Fig. 2. In seepage-solid potential, the normal attractive potential is applied at a distance and SB is applied instead for the repulsive interaction. Therefore, applying an accurate wall location is compromised, but the fluid atoms near the wall are most stable. Then, this is an ideal method for the fluid atom insertion while the liquid–solid interface structure is closely preserved. If the seepage solid is removed and the region becomes an insertion hole, a fluid-vacuum interface emerges. The free surface is less stable to maintain and has different properties than the solid-liquid. In the implementation, the interactions between the seepage atoms and the inserted fluid particle are calculated using the potential for a real solid and are closely monitored. When the particle is under the solid surface location (Zo in Fig. 1) or the net force by the collection of the seepage atoms is repulsive, the resulting repulsive force is inactivated and the SB is applied. When the net force becomes attractive, it is applied to the equations of motion. (The dotted line in Fig. 1 illustrates the location of the changing sign.)

The inserted particle is initially attracted by the liquid phase in the distance. When it reaches the solid–liquid interfacial region, the particle will be easily repelled until it finds a low-energy position in the dense, inhomogeneous population. Thus, SB also plays the role of forcing the particle to join the liquid phase. The SB is equivalent to increasing the momentum towards the liquid phase by twice the existing normal momentum.

Finally, the adequate distance between the inserted particle and dense liquid phase makes the insertion-process stable. This distance is analogous to the extra coordinate adopted in PIE, which also relaxes the strong force between the particles [16]. Conversely, the distance is based on a real coordinate here while the extra coordinate in PIE is an artificial one in the extended Hamiltonian.

3. Method

The simulations are conducted for two different states. In non-equilibrium molecular simulations, the simulation system is in contact with the vacuum on the top, where the fluid particles are out of bounds and do not return. When a particle drifts into the vacuum and gets lost, a new particle is inserted into the seepage-solid region at the bottom (Fig. 1). The total number of particles in the simulation system therefore remains constant. The box, called Tbox, on top of the seepage solid region with a size of 1σ, where the temperature is controlled by the Lowe-Andersen thermostat with the bath collision frequency Γ of 100 and cutoff distance R_T of 2 [24, 25]. Therefore, while the particle number, simulation volume, and system temperature (NVT) remain constant, there are mass fluxes into and out of the system at all times. After the initial equilibration period, a steady state is attained. In the second simulation type, the equilibrium molecular dynamics simulation is conducted with constant NVT.

The fluid interactions are modeled using the truncated and shifted Lennard-Jones 6-12 potential,

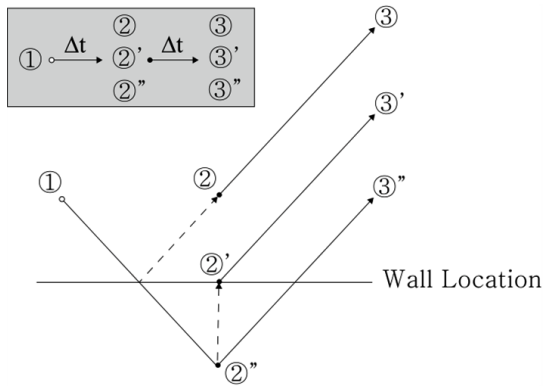

Fig. 2. Particle trajectories according to three different types of applications of wall condition.

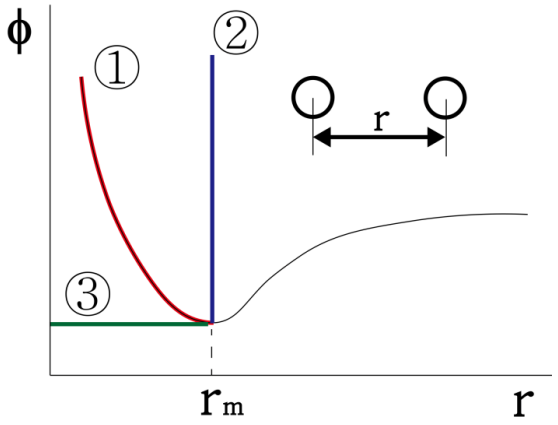

Fig. 3. Schematic of various interparticle potential: ① normal potential with a smooth strong repulsive potential, ② hard-sphere potential, ③ seepage-solid potential where soft-bounce is applied when $r < r_m$.

$$U_{LJts}(r)=\begin{cases}U_{LJ}(r)-U_{LJ}(r_c) & r<r_c\\ 0 \quad , \ otherwise\end{cases}, \tag{1}$$

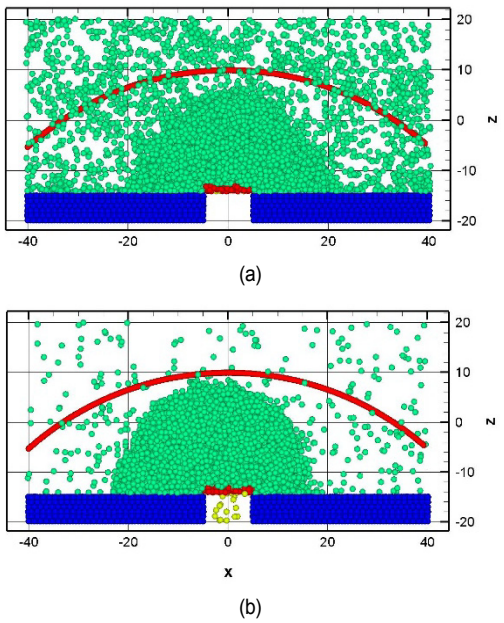

Fig. 4. Snapshots of the simulations of a drop on solid substrate: (a) the equilibrium evaporation; (b) the vacuum evaporation. The seepage-solid atoms are not shown for clarity. Blue particles are solid atoms, red particles are those inside the box for the thermostat application, yellow particles are those in the process of insertion, and green particles are the normal fluid atoms. The red line is the location of evaporation-flux measurement.

where

$$U_{LJ}(r)=4\epsilon\left[\left(\frac{r}{\sigma}\right)^{12}-\left(\frac{r}{\sigma}\right)^{6}\right]. \quad (2)$$

The cutoff length r_c is set at 6.5σ. The fluid of this potential can be regarded as argon. Then, σ is 3.4Å and $\frac{\epsilon}{k_B}=120K$ in real physical units. The initial positions of solid atoms are of the face-centered-cubic (FCC) lattice. The solid atoms interact with each other by harmonic potential,

$$U_{harmonic}(r)=\frac{1}{2}k(r-r_o)^2, \quad (3)$$

where r_o is the distance between the nearest atoms in the FCC lattice (111) and is 0.83σ. The spring constant k is set at 3042.3 ϵ/σ^2. The interaction between fluid and solid atoms is also modeled using the U_{LJts} potential where $\sigma_{fs}=1.19\sigma$ and $\epsilon_{fs}=0.42\epsilon$ are used. These model values are from the modeling of the collision interaction between Ar and Pt [26]. A layer of solid atoms at the bottom of the lattice is fixed in space. The solid atoms in the second layer from the lattice bottom is controlled by the Langevin equation,

$$m\ddot{x}+\gamma\dot{x}=f_{int}+F_{rand}, \quad (4)$$

where f_{int} is all the forces by the surrounding atoms, F_{rand} is the random force that satisfies the fluctuation-dissipation theorem and complies with the target temperature [27, 28]. The random force is drawn from a Gaussian distribution with zero mean and a standard deviation of $\sqrt{2\gamma k_B T/\delta t}$. The damping factor γ is given as 38.4 $(m\epsilon)^{1/2}/\sigma$. The equations of motion are integrated by using the velocity Verlet method [1]. A time step of 0.002 is used in the integration. The PBCs are applied to two horizontal directions.

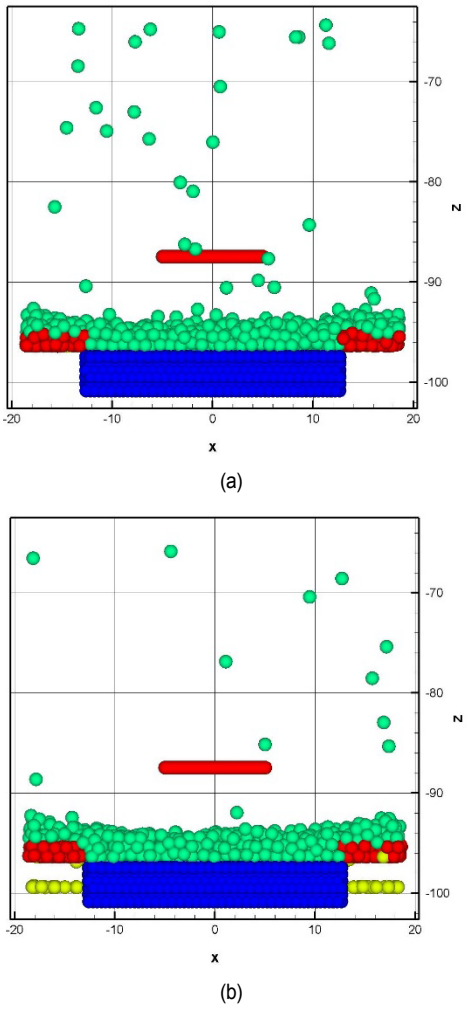

Fig. 5. Snapshots of the thin film simulations on solid substrate: (a) the equilibrium evaporation; (b) the vacuum evaporation. The seepage-solid atoms are not shown for clarity. The particle colors are classified the same as in Fig. 4.

4. Results

All of the results are presented in reduced units based on the LJ potential parameters. The insertion operation performance is tested for both thin film and drops on substrate systems and are shown to always be stable (Figs. 4 and 5). Fig. 6 shows the typical properties of an insertion operation. In this case, only a single particle participates in the insertion process. In Fig. 6(a), the inserted particle steadily progresses to the liquid–solid in-

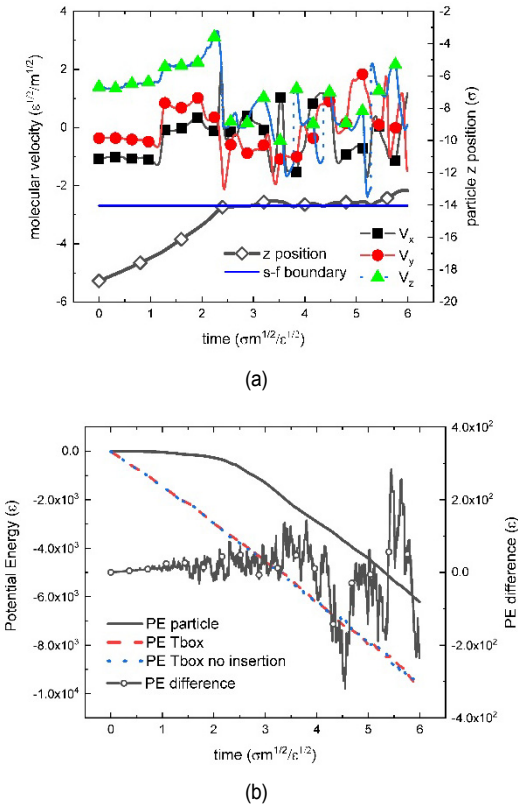

Fig. 6. Properties during the insertion operation of a single particle.

terface, passing through the seepage-solid region. The particle speed gradually increases due to the liquid phase attraction in the distance. When the particle reaches the interface, its progress suddenly becomes slow and the normal velocity to the interface becomes jittery. This is the process of the particle adjusting to the dense environment by strongly interacting with the liquid.

Whenever the normal velocity becomes negative, SB is applied so that a forward momentum is added by changing the velocity sign while keeping the particle position. After a period of stagnation, the particle finds its position where the potential energy due to solid atoms, normal and seepage alike, are minimal; then the particle progresses into a stable position in the liquid medium. Fig. 6(b) shows the progress of the potential energy (PE) during the insertion operation of a single particle. The PE's of the inserted particle and the particle in the Tbox are both monotonously decreasing. In fact, the PE of the particles in the Tbox without any insertion operation are also decreasing in the same manner (the blue dotted line in Fig. 6(b)). This is because the drop is in the state of vacuum evaporation and all the molecules in the drop are drawn outwards. The potential energy difference between the particles in the Tbox with and without the insertion operation reveals the disruption due to the insertion. The PE is quite disturbed when the inserted particle is at the interface and adjusting itself to the dense phase, and the disturbance level is an order less than the PE change. The overall integration of the motion equation

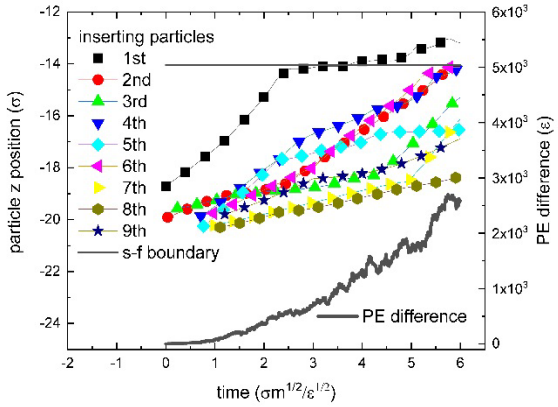

Fig. 7. Properties during the multiple particle insertion operations.

remains very stable.

Fig. 7 shows the case of multiple insertion particles (See also the snapshot, Fig. 4(b)). The particles are inserted sequentially, and the maximum rate of insertions are to be set. For example, only a density of at most 0.065 σ^{-3} is allowed in the seepage solid. Larger flux caused instability. In all the cases presented, the flux number under the density cap led to a stable steady state. The drop case required a larger mass influx than the thin film case. The PE by insertions in the Tbox steadily increased and the simulations do not become unstable.

Next, the mass-exchange technique is applied to the evaporation phenomena. The process of obtaining the evaporation coefficient in the MD simulation closely follows that in Ref. [29]. The mass flux of evaporating molecules, J^{evap}, is determined in a vacuum evaporating MD simulation [30, 31]. In the second set of simulations, the mass flux of outgoing molecules, J^{out}, is obtained in the same molecular system that is in contact with the bulk vapor phase. The component of the out-mass flux is then defined as,

$$J^{out} = J^{evap} + J^{ref}, \tag{5}$$

where J^{ref} is the mass flux of molecules reflected at the interface. The evaporation coefficient is obtained using the following definition,

$$\alpha_e = \frac{J^{evap}}{J^{out}_e}, \tag{6}$$

where the subscript *e* in J^{out}_e indicates the equilibrium state.

The evaporation in a thin flat film on a solid substrate is first investigated. As shown in Figs. 5(a) and (b), the liquid film wets the substrate while the solid-liquid interaction is modest. The seepage solids are located on both ends of the solid region. The evaporation is measured on the plane at the vapor phase, indicated as the red line in Figs. 5(a) and (b), by monitoring the number of particles passing through the plane. The simulations are conducted for the equilibrium evaporation state (Fig. 5(a))

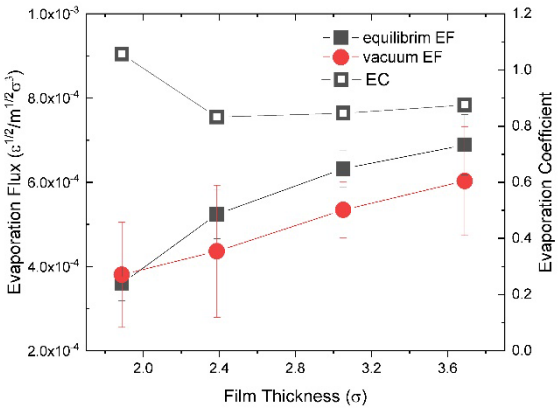

Fig. 8. Evaporation properties of thin films on a substrate.

and the vacuum evaporation state (Fig. 5(b)). The results are shown in Fig. 8. The evaporation fluxes of both simulations decrease with the film thickness, which is the initial thickness of the liquid film. This is the effect of the solid attraction potential that resists the escape of the fluid atoms from the film. Meanwhile, the evaporation coefficient remains almost constant in most cases except for the thinnest film case, because the film is so thin that the solid potential has a sizable influence over the film evaporation. However, the evaporation coefficient is rarely affected by the film thickness. This may not be the case for the strongly interacting solid where the influence of the solid would be farther reaching, which is to be studied in the future.

The sessile drop evaporation, another important class of evaporation phenomenon, is considered next using similar methods. The results snapshots are shown in Figs. 4(a) and (b). In this case, the seepage solid region is located at the center in the solid region. The red lines in the vapor phase again indicate the measurement planes for the evaporation flux. The center is at $\vec{x}_o = (0, 0, -50)$ with radius $R = 60$. Here, three cases of the fluid-solid interactions are considered: $\epsilon_{fs} / \epsilon_{ff} =$ 0.6, 0.8, and 1. As the interaction becomes weaker, the drop is in an increased partial-wetted state. The equilibrium evaporation flux does not appreciably change over the drop surface (Fig. 9(a)). However, the vacuum evaporation flux shows markedly uneven distribution (Fig. 9(b)). The evaporation near the contact line is clearly larger in the high-energy solid cases. The result is an uneven evaporation coefficient distribution (Fig. 9(c)). This indicates that there is a distinctively different mechanism of evaporation and condensation near the contact line. More detailed exploration on this phenomenon is again well worth a future study.

5. Conclusions

This study presents a simulation technique for inserting and deleting particles at the liquid–solid interface region. This technique involves selective activation of the interaction with the solid atoms and proves to be stable and efficient. It is quite useful in applying mass flux to the fluid system surrounded by

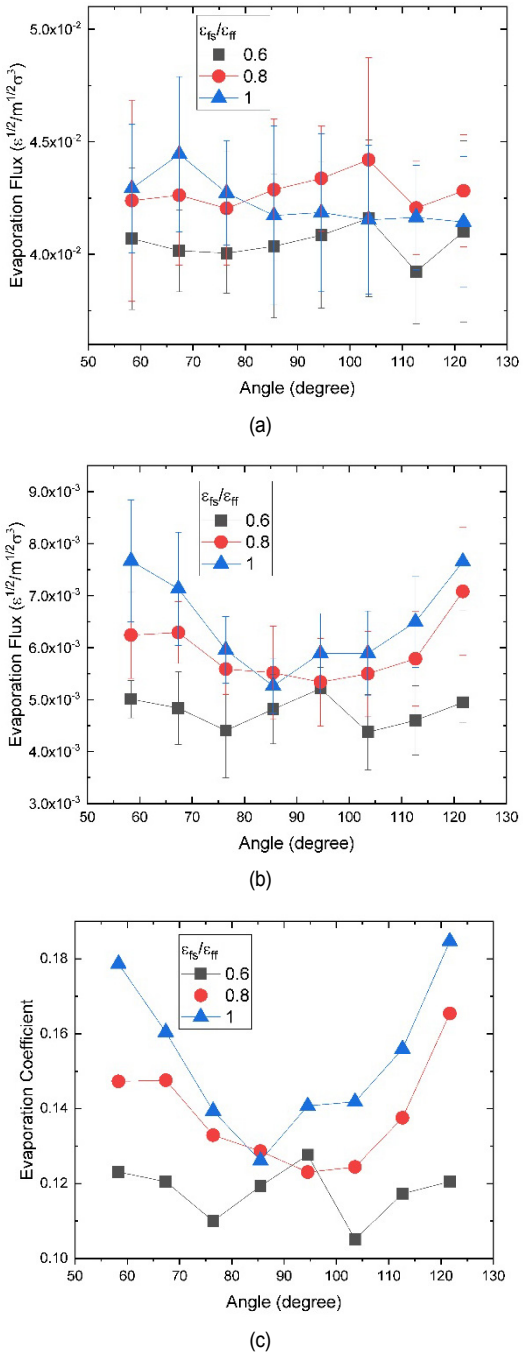

Fig. 9. Evaporation properties of sessile drops on a substrate: (a) equilibrium evaporation; (b) vacuum evaporation; (c) evaporation coefficient.

different material such as the solid substrate.

The evaporation phenomena of a thin film and a drop on a solid substrate are application examples where the fluid is bounded by solid and vapor phases on both sides and the fluid sources at the liquid–solid interfacial region maintain a steady state of evaporation and provide stationary evaporation data. As a result, the technique provides an evaporation-rate distribution near the contact line having a previously unavailable low fluctuation level.

In the thin flat film, the evaporation coefficient rarely changes, even for the films of only a-few-atomic-thicknesses. In the thinnest case, no elastic reflection on the interface is shown. The evaporation rate near the contact line on a high-energy solid substrate is larger than those far from the solid. This may indicate a different mechanism of evaporation and condensation at the contact line, which remains as a future study.

Acknowledgments

This work was supported by the Incheon National University Research Grant in 2016.

References

[1] M. P. Allen and D. J. Tildesley, *Computer Simulation of Liquids,* Oxford University Press (2017).

[2] D. C. Rapaport and D. C. R. Rapaport, *The Art of Molecular Dynamics Simulation*, Cambridge University Press (2004).

[3] G. S. Heffelfinger and F. Swol, Diffusion in Lennard-Jones fluids using dual control volume grand canonical molecular dynamics simulation (DCV-GCMD), *The Journal of Chemical Physics,* 100 (1994) 7548-7552.

[4] I. C. Brooks and M. Karplus, Deformable stochastic boundaries in molecular dynamics, *The Journal of Chemical Physics,* 79 (1983) 6312-6325.

[5] M. Berkowitz and J. A. McCammon, Molecular dynamics with stochastic boundary conditions, *Chemical Physics Letters*, 90 (1982) 215-217.

[6] T. Cagin and B. M. Pettitt, Grand molecular dynamics: A method for open systems, *Molecular Simulation*, 6 (1991) 5-26.

[7] R. M. Shroll and D. E. Smith, Molecular dynamics simulations in the grand canonical ensemble: Application to clay mineral swelling, *The Journal of Chemical Physics,* 111 (1999) 9025-9033.

[8] H. Eslami and F. Müller-Plathe, Molecular dynamics simulation in the grand canonical ensemble, *Journal of Computational Chemistry,* 28 (2007) 1763-1773.

[9] K. Mohamed and A. Mohamad, A review of the development of hybrid atomistic–continuum methods for dense fluids, *Microfluidics and Nanofluidics*, 8 (2010) 283-302.

[10] E. Flekkøy, G. Wagner and J. Feder, Hybrid model for combined particle and continuum dynamics, *EPL (Europhysics Letters)*, 52 (2000) 271.

[11] N. G. Hadjiconstantinou and A. T. Patera, Heterogeneous atomistic-continuum representations for dense fluid systems, *International Journal of Modern Physics C*, 8 (1997) 967-976.

[12] M. Mezei, Theoretical calculation of the liquid—Vapor coexistence curve of water, chloroform and methanol with the cavity-biased Monte Carlo method in the gibbs ensemble, *Molecular Simulation,* 9 (1992) 257-267.

[13] R. Delgado-Buscalioni and P. Coveney, USHER: An algorithm for particle insertion in dense fluids, *The Journal of Chemical Physics,* 119 (2003) 978-987.

[14] M. K. Borg, D. A. Lockerby and J. M. Reese, The FADE mass-stat: a technique for inserting or deleting particles in molecular dynamics simulations, *The Journal of Chemical Physics,* 140 (2014) 074110.

[15] J. Sablić, M. Praprotnik and R. Delgado-Buscalioni, Open boundary molecular dynamics of sheared star-polymer melts, *Soft Matter*., 12 (2016) 2416-2439.

[16] M. Han, Exchange of macromolecules and colloids in a dense medium: A molecular simulation method, *Journal of Computational Physics*, 395 (2019) 263-274.

[17] K. Signe and B. Dick, *Non-equilibrium Thermodynamics of Heterogeneous Systems*, World Scientific (2008).

[18] B. C. Garrett, G. K. Schenter and A. Morita, Molecular simulations of the transport of molecules across the liquid/vapor interface of water, *Chemical Reviews,* 106 (2006) 1355-1374.

[19] S. Fujikawa, T. Yano and M. Watanabe, *Vapor-liquid Interfaces, Bubbles and Droplets: Fundamentals and Applications*, Springer Science & Business Media (2011).

[20] N.-H. Kim, Enhancement of steam condensation on titanium corrugated tubes under vacuum condition, *Journal of Mechanical Science and Technology*, 33 (2019) 4023-4027.

[21] D. H. Shin, D. Y. Kim, C. K. Choi and S. H. Lee, Quantitative measurements of nanoparticle layer thicknesses near the contact line region after droplet drying-out, *Journal of Mechanical Science and Technology*, 33 (2019) 967-971.

[22] C. Cercignani, *Rarefied Gas Dynamics: from Basic Concepts to Actual Calculations,* Cambridge University Press (2000).

[23] Y. Sone, *Kinetic Theory and Fluid Dynamics Birkhauser*, Boston (2002).

[24] E. Koopman and C. Lowe, Advantages of a Lowe-Andersen thermostat in molecular dynamics simulations, *The Journal of Chemical Physics,* 124 (2006) 204103.

[25] C. Lowe, An alternative approach to dissipative particle dynamics, *EPL (Europhysics Letters)*, 47 (1999) 145.

[26] G. Q. Xu, S. L. Bernasek and J. C. Tully, Stochastic trajectory studies of small argon cluster scattering from Pt (111), *The Journal of Chemical Physics,* 88 (1988) 3376-3384.

[27] P. Yi, D. Poulikakos, J. Walther and G. Yadigaroglu, Molecular dynamics simulation of vaporization of an ultra-thin liquid argon layer on a surface, *International Journal of Heat and Mass Transfer*, 45 (2002) 2087-2100.

[28] J. C. Tully, Dynamics of gas–surface interactions: 3D generalized Langevin model applied to fcc and bcc surfaces, *The Journal of Chemical Physics*, 73 (1980) 1975-1985.

[29] T. Ishiyama, S. Fujikawa, T. Kurz and W. Lauterborn, Non-equilibrium kinetic boundary condition at the vapor-liquid interface of argon, *Physical Review E*, 88 (2013) 042406.

[30] T. Ishiyama, T. Yano and S. Fujikawa, Molecular dynamics study of kinetic boundary condition at an interface between argon vapor and its condensed phase, *Physics of Fluids*, 16 (2004) 2899-2906.

[31] T. Ishiyama, T. Yano and S. Fujikawa, Molecular dynamics study of kinetic boundary condition at an interface between a polyatomic vapor and its condensed phase, *Physics of Fluids*, 16 (2004) 4713-4726.

Minsub Han received his Ph.D. in Mechanical Engineering, majoring in Microscale Fluid Dynamics. His current interests include particle simulations applied to small-scale fluids and soft matter.